

# Adaptable Ultraviolet Reflecting Polymeric Multilayer Coatings of High Refractive Index Contrast

José Raúl Castro Smirnov, Masateru Ito, Mauricio Ernesto Calvo, Carmen López-López, Alberto Jiménez-Solano, Juan Francisco Galisteo-López, Paul Zavala-Rivera, Koichiro Tanaka, Easan Sivaniah,\* and Hernán Míguez\*

A synthetic route is demonstrated to build purely polymeric nanostructured multilayer coatings, adaptable to arbitrary surfaces, and capable of efficiently blocking by reflection a targeted and tunable ultraviolet (UV) range. Reflection properties are determined by optical interference between UV light beams reflected at the interfaces between polystyrene layers of different porosity and hence refractive index. As no dopant absorber intervenes in the shielding effect, polymer degradation effects are prevented. Alternated porosity results from the modulation of photochemical effects at the few tens of nanometers length scale, combined with the collective osmotic shock induced during the processing of the precursor diblock copolymer film. Experimental evidence of the application of this method to coat rough surfaces with smooth and conformal UV protecting films is provided.

a series of undesirable photoreactions promoted by the absorption of UV photons, which lead to the deterioration of their mechanical and optical properties. Polymers are usually transparent to part of the UV spectrum, so a commonly employed synthetic strategy to attain UV blocking films is based on embedding inorganic<sup>[3–7]</sup> or organic<sup>[8–10]</sup> UV absorbers within a polymeric matrix. The main drawback of this approximation is the short term durability of the shielding effect as a result of the photodegradation of either host, guest, or both, caused by the absorption of the same radiation from which protection is sought after.<sup>[11–13]</sup> Approaches based on flexible inorganic nanostructured multilayers that

## 1. Introduction

Research on polymer based films capable of shielding against ultraviolet (UV) radiation is nowadays intense as they are needed in a wide variety of sensitive environments for numerous applications.<sup>[1,2]</sup> Different organic materials, like plastic, wood, paper or textiles, and compounds, such as pigments or dyes undergo

efficiently reflect radiation in an arbitrary spectral range as a result of interference effects, rather than by absorption, present a promising alternative route worth to be explored.<sup>[14–17]</sup> Unfortunately, a similar approach based on the alternation of polymeric films exclusively is not feasible since the refractive index contrast typically achieved is so small that a large number of layers is required to reach a significant reflectance, and only in a narrow spectral range.<sup>[18,19]</sup> The use of all-polymeric materials of high refractive index contrast to build multilayer back reflectors or UV shields will also be an advantage in the field of flexible and polymeric solar cells, in which some approaches based on inorganic materials have already been developed.<sup>[20,21]</sup> Very recently, some of us proved that a porous stratified structure displaying strong reflection peaks in the UV range can be attained from a block copolymer (BCP) film.<sup>[22]</sup> In particular, it was demonstrated that a film made of a diblock copolymer containing polystyrene (PS) and polymethyl methacrylate (PMMA), in brief [poly(styrene-block-methyl methacrylate) PS-*b*-PMMA], can be used as starting material to attain ordered porous multilayers through a process that involves collective osmotic shock (COS). The final structure shows alternate dense and porous layers, with significant refractive index contrast, which endow it with photonic crystal properties in the UV range. At that moment, the appearance of the layered structure was hypothetically attributed to dynamic effects during the COS process occurring over ordered arrangements of isolated PMMA spheres embedded in a cross-linked PS matrix in the starting slab, which had previously been subjected to thermal and UV annealing processes. Further studies, herein reported, have demonstrated that the mechanism of formation of the porous layered structure is different to that originally

Dr. J. R. C. Smirnov, Dr. M. E. Calvo,  
Dr. C. López-López, A. Jiménez-Solano,  
Dr. J. F. Galisteo-López, Prof. H. Míguez  
Instituto de Ciencia de Materiales de Sevilla  
Consejo Superior de Investigaciones  
Científicas-Universidad de Sevilla  
Américo Vespucio 49, Sevilla 41092, Spain  
E-mail: h.miguez@csic.es

Dr. M. Ito, Prof. K. Tanaka, Dr. E. Sivaniah  
Institute for Integrated Cell-Material Science  
Kyoto University  
Kyoto 606-8501, Japan  
E-mail: e.sivaniah@icems.kyoto-u.ac.jp

Dr. P. Zavala-Rivera  
Departamento de Ingeniería Química y Metalurgia  
Universidad de Sonora  
Blvd Luis Encinas S/N, Hermosillo, Sonora, CP 83000, Mexico

The copyright line of this paper was changed 23 September 2015 after initial publication.

This is an open access article under the terms of the Creative Commons Attribution-NonCommercial License, which permits use, distribution and reproduction in any medium, provided the original work is properly cited and is not used for commercial purposes.

DOI: 10.1002/adom.201500209



proposed. These findings have opened the way to precise control of the photonic crystal properties of the film as well as to its formation on arbitrary surfaces.

In this full paper, we present a synthetic route to prepare purely polymeric photonic crystal coatings displaying intense UV reflections of tunable wavelength and adaptable to surfaces with arbitrary roughness. By unveiling the mechanism of formation of the structure of layers of alternate porosity present in the film, we discover at the same time a method to finely tune the position of the reflectance peak in the UV range, enhancing the functionality of these coatings. We provide evidence that shows that periodicity is a direct consequence of the formation of a standing electromagnetic wave generated by thin film interference during the UV irradiation stage of the process. Standing waves impose a periodic pattern of PMMA degradation and PS crosslinking at the nanoscale, hence determining the periodicity of the porous structure that arises after acid etching, regardless the geometrical constants and number of sphere lattice planes in the starting film. These results constitute, as far as we know, the first demonstration of spatial modulation of UV induced photochemical effects in block copolymers. In this regard, the periodically stratified porous structures, whose formation procedure is herein discussed, may be considered as the consequence of a sort of bulk UV lithography processing of block copolymers. Our hypothesis is supported by full vector wave theoretical calculations of the electromagnetic field intensity distribution across the diblock copolymer film.

## 2. Results and Discussion

The possibility to control the photonic crystal properties of purely polymeric coatings resulted from the understanding and control of the mechanism of formation of alternate porous and dense layers in BCP films deposited on a flat substrate. In order to analyze it, we prepared a series of films on  $2.5 \times 2.5 \text{ cm}^2$  silicon wafers by spin-coating a solution of PS-*b*-PMMA of different total molecular weight ( $M_w = M_{w,PMMA} + M_{w,PS}$ ) but with approximately the same ratio  $\phi = M_{w,PMMA}/M_{w,PS}$  ( $0.13 < \phi < 0.17$ ). Films were subsequently treated thermally to stabilize a 3D lattice of nonconnected PMMA spheres in a matrix of PS. Using a similar  $\phi$  ratio ensures that all samples will have a similar periodic arrangement at the nanoscale, which is expected to be face centered cubic (fcc),<sup>[23]</sup> while the different  $M_w$  will give rise to very different sphere size and hence interplanar distance. Hence, PS-*b*-PMMA slabs were prepared using with  $M_{w,PS} = 71 \text{ kDa}$  ( $\phi = 0.16$ ),  $81 \text{ kDa}$  ( $\phi = 0.15$ ),  $126 \text{ kDa}$  ( $\phi = 0.16$ ),  $135 \text{ kDa}$  ( $\phi = 0.14$ ),  $295 \text{ kDa}$  ( $\phi = 0.15$ ), and  $1000 \text{ kDa}$  ( $\phi = 0.14$ ). As one of the components is stiffer than the other at room temperature, atomic force microscopy (AFM) is a useful technique to reveal topological and compositional information of these films.<sup>[24]</sup> The mean center to center distances,  $d$ , estimated from AFM image analysis (see the Supporting Information, Figures S1 and S2) are  $d = 30 \text{ nm}$ ,  $d = 40 \text{ nm}$ ,  $d = 65 \text{ nm}$ , and  $d = 90 \text{ nm}$  for samples of  $M_{w,PS} = 71.5 \text{ kDa}$  ( $\phi = 0.16$ ),  $M_{w,PS} = 81 \text{ kDa}$  ( $\phi = 0.15$ ),  $M_{w,PS} = 126 \text{ kDa}$  ( $\phi = 0.16$ ), and  $M_{w,PS} = 135 \text{ kDa}$  ( $\phi = 0.14$ ), respectively. On the other hand, samples attained from PS-*b*-PMMA of  $M_{w,PS} = 295 \text{ kDa}$  ( $\phi = 0.15$ ) or  $M_{w,PS} = 1000 \text{ kDa}$  ( $\phi = 0.14$ ) present weak first

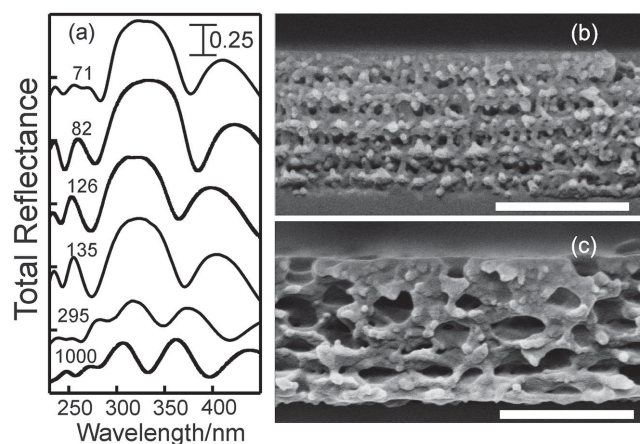


**Figure 1.** a) Total reflectance spectra measured after treatment for PS-PMMA diblock copolymers with different  $M_w$ . We label each spectrum with the corresponding molecular weight (in kDa) of the polystyrene fraction. As spectra have been vertically shifted for the sake of clarity, a scale bar corresponding to absolute reflectance of 0.25 is also shown as an inset. FESEM cross section micrographs of porous multilayers prepared from films of PS-PMMA of different  $M_w$ : b) 126 kDa and c) 295 kDa. Scale bar is 500 nm in both images.

neighboring correlations and less long range order, with estimated mean distances of 280 and 500 nm, respectively. These results are in good agreement with those previously attained by high resolution transmission electron microscopy.

All these samples were exposed to the dose ( $8 \text{ J cm}^{-2}$ ) of UV light ( $\lambda = 254 \text{ nm}$ ) necessary to attain a periodic porous multilayer, as reported in ref. [16]. The effect of this treatment is to both trigger the crosslinking of PS and degrade the PMMA to low molecular weight oligomers. Finally, films were immersed in acetic acid, a solvent of PMMA that at the same time is capable of diffusing through cross-linked PS without dissolving it.<sup>[25]</sup> As the acetic acid reaches the PMMA through the PS matrix, which acts as a semi-permeable barrier for solvent transfer, osmotic pressure builds up due to swelling of the spherical domains, which deform anisotropically. Thinning of the PS walls in between spheres eventually leads to their rupture and the formation of layers with large pores supported by PS columns, separated from perforated layers of higher density.

As it can be seen in **Figure 1a**, the structures of the coatings attained from PS-*b*-PMMA of  $M_w$  71, 82, 126, and 135 kDa present strong (up to 80%) reflectance peaks in the UV region that can be unambiguously attributed to Bragg diffraction effects arising from a relatively strong periodic modulation of refractive index ( $n_L = 1.23$  and  $n_H = 1.52$ , for each pair of consecutive layers) along one spatial dimension that takes place in distances of the order of a hundred nanometers. The cross section of these structures displays a periodic alternation of low and high porosity layers, as can be seen in field emission scanning electron microscopy (FESEM) image displayed in **Figure 1b**. A full description of the pore size distribution of the two types of layers present in these structures was realized by specular reflectance porosimetry<sup>[26]</sup> and can be found in the Supporting Information (please see Figures S3–S5 and related content). Four samples (71, 82, 126, and 135 kDa) present reflection peaks at the exact same spectral position ( $\lambda \approx 320 \text{ nm}$ ) regardless of the PMMA

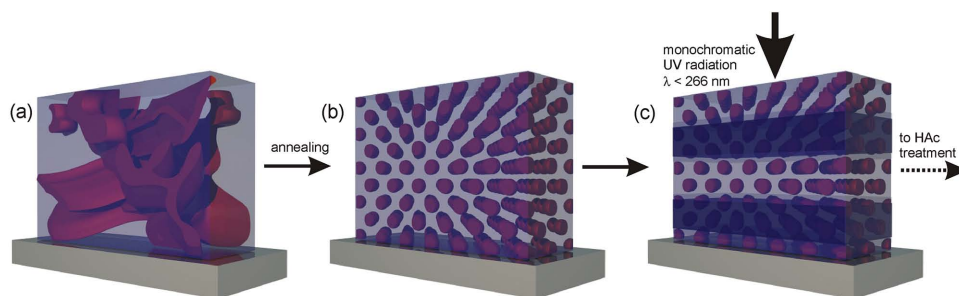


**Figure 2.** Scheme of the sequential process that BCP suffers a) room temperature deposition, b) bcc packing segregation of PMMA spheres after annealing, c) interference fringes located within the BCP stack resulting from UV illumination.

sphere size achieved in the segregated phase, in good agreement with the observation of an identical value of the periodicity in the FESEM images (Figure S6a–d, Supporting Information). No periodic distribution of pores is found in those films made with PS-*b*-PMMA of the largest  $M_w$  employed, 295 and 1000 kDa (Figure 1c and Figure S6f, Supporting Information), although AFM images reveal that phase separation has also occurred in those samples (see Figure S1, Supporting Information). Some degree of layering is also observed in these cases, but the rupture of large PMMA spheres by COS gives rise to an optically disordered system that displays no Bragg peak.

An explanation for these effects can be found in the particular field distribution of UV radiation that takes place within the film during processing. The irradiation source employed is a 2 mm diameter fluorescent tube located at 80 mm from the sample; hence UV light reaching the sample surface can be approximated as plane waves. All samples employed for this study have the same initial thickness ( $420 \pm 10$  nm). So, a similar spatial distribution of UV light field intensity is expected within all of them upon irradiation. In **Figure 2** we show a scheme of the herein proposed UV bulk lithography process taking place in the block copolymer prior to the soaking in acetic acid. First, the BCP is deposited at room temperature onto a silicon substrate (Figure 2a). After annealing, PMMA spheres are ordered in a face centered orthorhombic lattice (Figure 2b) as has been previously shown by grazing incidence small-angle X-ray scattering.<sup>[22]</sup> Under UV irradiation, a low and high UV field intensity fringe pattern is formed resulting from the standing wave generated by thin layer interference (Figure 2c).

In **Figure 3a** we show the specular reflectance spectra of the different diblock copolymer films employed as starting materials. The analysis of the interference fringes observed confirms that their average refractive index and thickness is approximately the same in all cases. Figure 3b displays the spatial distribution of the square of the electric field,  $|E|^2/|E_0|^2$ , for light of wavelength  $\lambda = 254$  nm impinging normally to the film deposited on silicon. Calculations were carried out using a code based on a vector wave transfer matrix method written in MatLab<sup>[27]</sup> using as inputs real and imaginary parts

of the dielectric constant attained by fitting the measured total reflectance and total transmittance of the film supported onto a quartz substrate, following a procedure described elsewhere.<sup>[28]</sup> The extinction coefficient of the BCP film is 0.0056 at  $\lambda = 254$  nm. The spatial profile of  $|E|^2/|E_0|^2$  is a consequence of the formation of a standing wave in the PS-*b*-PMMA film as a result of the interference between beams partially transmitted and reflected at the air–polymer and polymer–silicon interfaces. This gives rise to regions of low and high UV intensity illumination periodically distributed along the film cross section. This results in a spatial modulation in the degradation of PMMA and cross-linking of PS along the film normal, which should in turn modulate the collective osmotic shock process. So, as  $|E|^2/|E_0|^2$  describes a complete period in  $\approx 75$  nm, each one comprising a pair of low and high intensity fringes, and since the film thickness is 420 nm, around 11 layers (five and a half periods) of different microstructure should in principle be expected as a result of such modulation. UV induced photochemical effects on the COS poration process should be minimal in regions in which the  $|E|^2/|E_0|^2$  profile presents minima; such effects should be enhanced where  $|E|^2/|E_0|^2$  is around its maxima. This coincides well with the FESEM analysis of the cross sections of films prepared using PS-*b*-PMMA of  $M_{w,PS}$  71, 82, 126, and

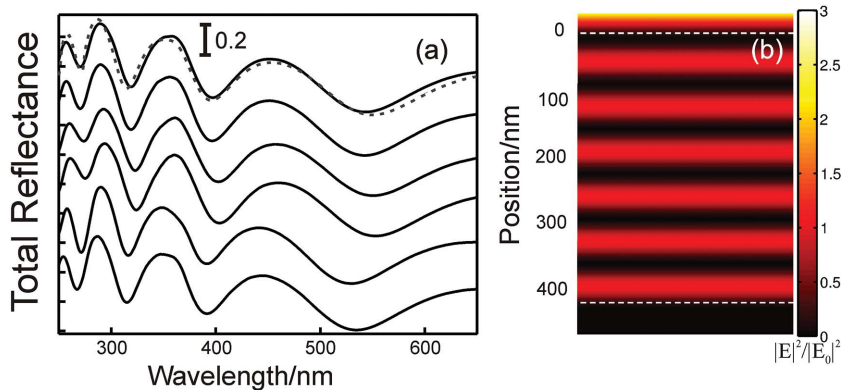


**Figure 3.** a) Total reflectance spectra for samples prepared with PS-*b*-PMMA with  $M_{w,PS}$  of 71, 81, 126, 135, 296, and 1000 kDa (spectra from above to below, black lines). A theoretical spectrum calculated for a PS-*b*-PMMA film is included (grey dashed line). As spectra have been vertically shifted for the sake of clarity, a scale bar corresponding to absolute reflectance of 0.5 is also shown as an inset. b) Spatial distribution along the cross section (Y axis) of the square of the UV ( $\lambda = 254$  nm) electric field represented for a PS-PMMA film with a thickness of 420 nm deposited on silicon substrate. White dashed lines represent film interfaces. Position at 0 nm represents the interface between air and PS-PMMA film.

135 kDa, as it can be seen in Figure 1b,c and Figure S6, Supporting Information. The final thickness of the porous multilayers in the FESEM images is larger than the initial 420 nm of the untreated film due to the expansion of the layers upon the out of plane swelling effect of collective osmotic shock.

Interestingly, those coatings in which the PMMA sphere size is much larger than the modulation (PS-*b*-PMMA of  $M_w$  295 and 1000 kDa), and for which no Bragg mirror properties were attained, show no periodic layering under the FESEM but just very large and irregular pores evenly distributed along the cross section. There are two possible reasons why the formation of a regular multilayer of modulated pore size is prevented. Either the thermal annealing is not capable of ordering the spheres in the first place due to the large block copolymer molecular weight, or the disorder is introduced by the acetic acid etching process when dissolving the PMMA, as now the same sphere should present regions with different degrees of depolymerization as a consequence of the spatial modulation of the UV induced photochemical effects introduced by the electromagnetic field distribution.

Hence the model herein proposed based on the distribution of the UV light field within the PS-*b*-PMMA films accounts both qualitatively and quantitatively for the formation of a periodic stratified structure of pores, as long as the PMMA spheres present in the slab are not too large compared to the period of the  $|E|^2/|E_0|^2$  profile. This period is 75 nm while sphere diameters estimated from our AFM image analysis are  $\approx 20$  nm ( $M_{w,PS} = 71.5$  kDa), 25 nm ( $M_{w,PS} = 81$  kDa), 40 nm (126 kDa), and 55 nm (135 kDa), for samples exhibiting a multilayered structure and photonic crystal properties, and 170 nm (295 kDa) and 300 nm (1000 kDa), for those showing no stratified ordering of pores, in agreement with our hypothesis. Furthermore, it also explains other previous observation, such as the absence of any periodicity when BCP films are exposed to a very high UV dose, since the regions of minimum  $|E|^2/|E_0|^2$  would then present enough PMMA depolymerization and PS stabilization as to behave just like the more intensely illuminated ones.<sup>[29]</sup> Also, it explains why the exposure time required is longer for those systems in which a less reflective substrate is employed, as the intensity of the high  $|E|^2/|E_0|^2$  fringes depends on that parameter. Interestingly, the absorbance spectrum of the film taken after the immersion in acetic acid shows bands that can be assigned to PS and PMMA chains, indicating that PMMA is only partially removed from the structure (see Figure S7, Supporting Information). Please notice that this description explains one striking feature of the periodic layered structures attained by COS reported in ref. [22],

which is that the number of periods in the stack was half of the number of sphere lattice planes present in the starting materials. This effect was hypothesized as the outcome of alternate layers of spheres being deformed in different extent, which would cause that half the sphere planes gave rise to perforated layers and the other half to columns. This postulate is nevertheless incompatible with the experimental observations herein presented.

A major implication of this finding is the possibility to finely tune the spectral position of the optical Bragg peak displayed by the porous multilayers by means of changing the angle of incidence on the sample of the UV light employed to process the BCP film. In order to attain a precise control, we employed a UV laser emitting at a wavelength of 266 nm, at which the photoinduced chemical degradation of PMMA and cross-linking of PS still occurs, to shine thermally treated precursor BCP films at different angles of incidence with respect

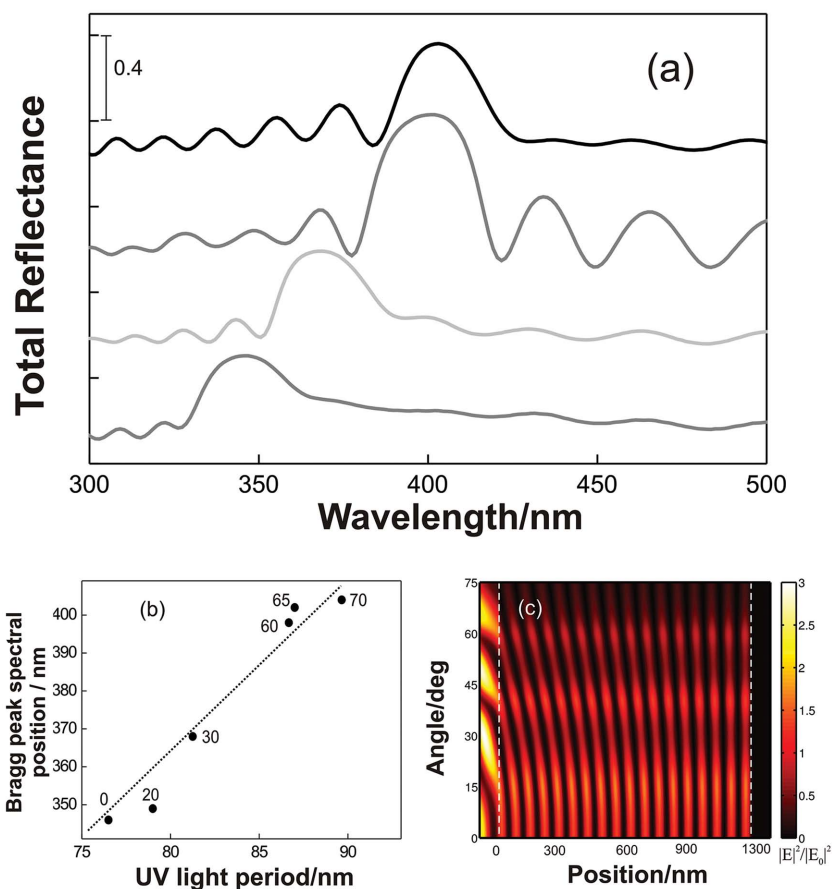


**Figure 4.** a) Total reflectance spectra for samples prepared with PS-*b*-PMMA with  $M_{w,PS}$ , 81 at different incident angles,  $\alpha$ , (in degrees).  $\alpha = 0^\circ$  grey solid line,  $\alpha = 30^\circ$  light grey solid line,  $\alpha = 60^\circ$  dark grey solid line and  $\alpha = 70^\circ$  black solid line. As spectra have been vertically shifted for the sake of clarity, a scale bar corresponding to absolute reflectance of 0.4 is also shown as an inset. b) Spectral position of the Bragg peak obtained through the UV illumination ( $\lambda = 266$  nm) at different incident angles (indicated as a number near the point) versus the period of UV light inside BCP film. c) Spatial distribution along the cross section (X axis) of the squared UV electric field calculated for a PS-PMMA film with a thickness of 1300 nm deposited on silicon substrate as a function of the angle of incidence (Y axis). White dashed lines represent film interfaces. The vertical white dashed lines indicate the interfaces between air and PS-PMMA ( $x = 0$  nm) and PMMA-silicon ( $x = 1300$  nm).

to the surface normal. The more oblique the incidence is, the longer the path travelled by light beams within the film; hence a source with long coherence length, such as a laser, was required to achieve a well-defined pattern of modulated light intensity within the film for a wide range of angles of incidence. The specular reflectance spectra of samples prepared using different angles of incidence of the UV laser beam are plotted in **Figure 4a**. A fine control over the position of the reflectance maximum is achieved in the wavelength range comprised between 350 and 400 nm for samples irradiated using a UV laser beam impinging in the angular range comprised between  $0^\circ$  and  $70^\circ$ . For the sake of clarity, in **Figure 4b** we plot the spectral position of the reflectance maximum against the period of the UV light pattern attained at 266 nm in the 1300 nm thick BCP film. As expected from Bragg law, there is a linear correlation between the spectral position of these peaks and the estimated period of the UV light fringe distribution pattern attained

at each angle of irradiation. The calculated evolution of the UV light intensity pattern along the cross section of the 1330 nm thick precursor BCP film as the angle of incidence increases is shown in **Figure 4c**. The expected number of periods decreases as the angle of incidence is larger. So, as the swelling effect of the collective osmotic shock gives rise to samples of comparable final thickness, the final period of the porous layered structure grows with the angle of incidence of UV light during treatment, and consequently the Bragg peak gradually red-shifts. In addition, our fittings (**Figure S8**, Supporting Information) indicate that the periodicity in the final multilayers ranges between 124 and 147 nm, which corresponds to a period in the UV light intensity fringe pattern between 76 and 90 nm in the precursor film, respectively. In all cases, reflectance maxima are above 55%. Variations observed between the different samples are explained by the effect of the different lattice terminations that result from the particular UV field distribution in each case. **Table S1** (Supporting Information) includes the values obtained from the fittings of the reflection spectra obtained at different incidence angle. It should be noted that the porosities of each layer obtained at different angles are comparable. This feature means that the angular incidence has a negligible effect on the refractive index of each layer, but a significant one on the lattice parameter (i.e., layer thickness).

The UV-interference correlated collective osmotic shock effect herein reported also provides a means to coat a corrugated surface with a UV protecting polymeric film. In order to prove this, we deposited a film of PS-*b*-PMMA onto an unpolished silicon substrate. Unpolished wafers surfaces have a topology characterized by extended flat regions tilted with respect to each other. Deposition by spin-coating creates a polymer coating that presents a flat outer surface to incident light and a corrugated inner one against the substrate. The UV interference field distribution in such cases, are primarily parallel to the substrate/BCP interface and not the BCP/air interface, as shown

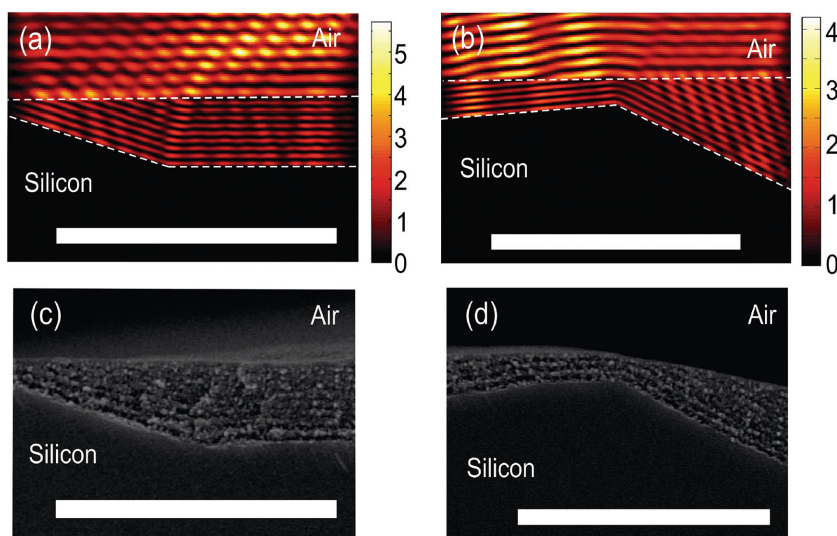


**Figure 5.** a,b) Total field intensity calculated for systems having the shape extracted from SEM images of samples depicted in (c) and (d) respectively. Air/polymer and polymer/silicon interfaces are indicated by dashed white lines in the simulations. Scale bars correspond to 3  $\mu\text{m}$  in all cases.

in the  $|E|^2/|E_0|^2$  profiles displayed in **Figure 5a,b**. In this case, field intensity patterns have been calculated using a commercial code (Lumerical) based on finite-difference-time-domain (FDTD) whose full details are given in the Experimental Section. After thermal and UV processing and acetic acid etching, periodic alternation between porous and dense layers occurs parallel to the flat silicon surfaces, as shown in **Figure 5c,d**, rather than to the flat top surface. These pictures allow us to confirm that the observed layering replicates the calculated spatial profile of  $|E|^2/|E_0|^2$  in the precursor PS-*b*-PMMA film. On the contrary, when dynamically variable angle of incidence of UV light coming from a low coherence source is employed, the uniform spread of field intensity gives rise to a film in which no periodic layered structure of pores is observed (**Figure S9**, Supporting Information).

A final question we addressed is the interplay between the existing order of spheres thermally induced when phases are segregated in the precursor BCP film and that imposed by UV light interference. A detailed description of this study is provided in the Supporting Information (please see **Figure S10**). Our analysis shows that, although ordering in the starting film is not mandatory to achieve a periodic multilayer, as the presence of alternate porous and dense layers is determined by the spatial modulation of the photochemical processes induced by UV light, it is indeed necessary to attain a well-defined interface between such regions. This is of particular relevance for potential applications of these coatings as reflectors in the ultraviolet B region of the spectrum ( $280 \text{ nm} < \lambda < 315 \text{ nm}$ ), as the intensity and spectral width of the peak depend strongly on the interface between adjacent layers of different refractive index.

The purely polymeric photonic crystal we herein present shows a high dielectric constant contrast between the alternated porous layers (1.52 vs 1.23). It is actually hard to find in the literature such a high contrast in periodic structures based only on polymers. As this contrast determines the width of the photonic

band gap and the scattering strength of the structure, our films allow us to obtain reflectance peaks with a full width at half maximum (FWHM) of 20% (estimated as the gap to midgap ratio) and of more than 80% reflectance with only seven bilayers. Please notice that these values are well above those previously reported for purely polymeric optical multilayers in which 25 bilayers are needed to reach 60% reflectance in a spectral range of 10 nm (gap to midgap ratio of around 2%).<sup>[18]</sup> Interestingly, the spectral range that is most harmful to skin coincides in both position and width with the reflectance peak displayed by our UV reflecting polymeric films, as the action spectrum of UV-induced genotoxicity in epithelial cells presents a maximum around  $\lambda \approx 310$  nm with a FWHM of 25 nm.<sup>[30,31]</sup> This spectrum could be matched efficiently by that of our porous photonic coatings, whose FWHM is approximately 70 nm at a wavelength of 320 nm. This is an example of the sort of applications the films herein proposed could give rise to.

### 3. Conclusions

From an applied perspective, the most relevant conclusion of the work herein reported is that it is possible to develop conformal UV reflecting coatings made of purely polymeric compounds adaptable to nonflat substrates. The periodicity, and thus the photonic crystal properties, of the porous multilayer can be precisely tuned by changing the angle of incidence of the UV light during the processing of the precursor film. From a more fundamental point of view, the key finding is that spatial modulation of UV induced photochemical effects, which arise from thin film interference effects, plays a key role in the formation of periodically nanostructured multilayers from block copolymer films undergoing collective osmotic shock. From this new hypothesis several corollary outcomes were predicted and proven. Overall, the experimental evidence herein reported constitutes, as far as we know, the first example of UV bulk lithography in heteropolymers. These results may serve as starting point to design more complex patterns within block copolymers by means of 3D laser interference in a similar way to what has been done with homopolymers.

### 4. Experimental Section

All poly(styrene-*block*-methyl methacrylate) [PS-*b*-PMMA] were purchased from Polymer Source Inc. (Dorval, Canada). PS-*b*-PMMA copolymers were selected with molecular weights of polystyrene (PMMA/PS volume fraction,  $\phi$ , and polydispersity index, PDI, between brackets) of 71 kDa ( $\phi = 0.16$ , PDI = 1.17), 81 kDa ( $\phi = 0.15$ , PDI = 1.08), 126 kDa ( $\phi = 0.16$ , PDI = 1.09), 135 kDa ( $\phi = 0.14$ , PDI = 1.08), 295 kDa ( $\phi = 0.15$ , PDI = 1.35), and 1000 kDa ( $\phi = 0.14$ , PDI = 1.20). These fractions values are needed in order to produce PMMA sphere phase segregation. Appropriate amounts of each polymer were dissolved in toluene to reach a 6 (wt%/vol%) concentration and deposited by spin coating onto silicon or quartz substrates. Spin coating final rotation speed and acceleration were adjusted in each BCP solution to attain the same thickness in all PS-*b*-PMMA films. Films were annealed during 6 h at 180 °C under N<sub>2</sub> atmosphere. After irradiation step (see the next section) samples were immersed during 30 min in glacial acetic acid (Merck) to dissolve the fraction of PMMA producing the osmotic shock process.

**Irradiation Experiments:** Samples were irradiated in a crosslinker (CX-2000, UVP Ltd., Cambridge) for 20 min. Four 8 W thin light tubes emitted 254 nm light. Quasi-normal incidence was achieved by placing the samples on the chamber floor, which is located at 80 mm from the source. Experiments whose results are presented in Figure S9 (Supporting Information) were carried out using an oscillating holder that varies the incident angle from 0° to 60° at a frequency of 0.5 Hz. In all cases, the energy received by the samples is adjusted to 8 J cm<sup>-2</sup>.

A fourth harmonic Nd:YAG laser (DIVA II 266HP) was used as a laser light source. It has a pulse frequency of 20 Hz and FWHM of 10.9 ns. The light was polarized in the plane of incidence (p-polarization). The beam size was changed by a double-convex lens, so that the lens-sample distance was greater than the focal distance; the final beam incident on the block copolymer films was enlarged to a 7 mm spot diameter so the incident beam intensity on the films was 16 mW cm<sup>-2</sup> and total energy irradiated during experiments was 4 J cm<sup>-2</sup>.

**Optical and Structural Characterization:** Total reflectance (RT) and total transmittance (TT) spectra were obtained using a UV-visible scanning spectrophotometer (Shimadzu UV-2101PC) attached to an integrating sphere. FESEM images of the multilayers films deposited onto silicon were taken by using a microscope Hitachi 5200 operating at 5 kV. Samples were immersed in liquid nitrogen before they were cut to analyze the cross section. A thin layer consisting in 5 nm of gold was sputtered on samples to avoid charging effects in the FESEM observation. AFM images were acquired with an AFM Park Systems XE-100. Images were analyzed using ImageJ software (<http://imagej.nih.gov/ij>).

**Theoretical Analysis:** Analytical calculations were performed to obtain the light field intensity patterns plotted in Figure 3 using a code developed in MatLab and based on a vector wave transfer matrix approach, as described in ref. [20]. Real and imaginary parts of the refractive index of the different materials involved in all the simulations are provided in the Supporting Information (please see Figure S11). The interference patterns in Figure 4a,b were simulated with a 3D calculation using a commercial FDTD code. The simulated structure was designed using the cross section obtained from the SEM images shown in Figure 4c,d. In the simulation the polymer thickness was assumed to be that of the un-swelled system ( $\approx 80\%$  of the final thickness) and the irradiation beam was a plane wave with wavelength 254 nm incident normally on the polymer/air interface. A sufficiently fine grid ( $\geq 20$  points per wavelength) and long simulation times ( $\geq 1$  ps) were used in order to correctly simulate the structures.

### Supporting Information

Supporting Information is available from the Wiley Online Library or from the author.

### Acknowledgements

The research leading to the results has received funding from the European Research Council under the European Union's Seventh Framework Programme (FP7/2007-2013)/ERC Starting Grant agreement no. 307081 (POLIGHT), the Spanish Ministry of Economy and Competitiveness under grant MAT2011-23593, the repatriation project (232100) from CONACYT Mexico, and the Japan Science and Technology Agency Sakigake program (Innovative Functional Materials by Hyper-nano-space Design). AFM and FESEM characterization were performed at CITIUS, and we are grateful for its support.

Received: April 19, 2015

Revised: June 16, 2015

Published online: August 31, 2015

- [1] M. Zayat, P. Garcia-Parejo, D. Levy, *Chem. Soc. Rev.* **2007**, *36*, 1270.
- [2] M. E. Calvo, J. R. Castro-Smirnov, H. Míguez, *J. Pol. Sci. B: Pol. Phys.* **2012**, *50*, 945.
- [3] M. M. Demir, K. Koynov, U. Akbey, C. Bubeck, I. Park, I. Lieberwirth, G. Wegner, *Macromolecules* **2007**, *40*, 1089.
- [4] G. S. Liou, P. H. Lin, H. J. Yen, Y. Y. Yu, T. W. Tsai, W. C. Chen, *J. Mater. Chem.* **2010**, *20*, 531.
- [5] Y. Tu, L. Zhou, Y. Z. Jin, C. Gao, Z. Z. Ye, Y. F. Yang, Q. L. Wang, *J. Mater. Chem.* **2010**, *20*, 1594.
- [6] L. Mazzocchetti, E. Cortecchia, M. Scandola, *ACS Appl. Mater. Interfaces* **2009**, *1*, 726.
- [7] D. Koziej, F. Fischer, N. Kränzlin, W. R. Caseri, M. Niederberger, *ACS Appl. Mater. Interfaces* **2009**, *1*, 1097.
- [8] J. Keck, M. Roessler, C. Schroeder, G. J. Stueber, F. Waiblinger, M. Stein, D. Legourrierec, H. E. A. Kramer, H. Hoier, S. Henkel, P. Fischer, H. Port, T. Hirsxh, G. Rytz, P. Hayoz, *J. Phys. Chem. B* **1998**, *102*, 6975.
- [9] B. Mahltig, H. Bottcher, K. Rauch, U. Dieckmann, R. Nitsche, T. Fritz, *Thin Solid Films* **2005**, *485*, 108.
- [10] H. Cui, M. Zayat, P. García Parejo, D. Levy, *Adv. Mater.* **2008**, *20*, 65.
- [11] M. Nowick, A. Richter, B. Wolf, B. H. Kaczmarek, *Polymer* **2003**, *44*, 6599.
- [12] R. Yang, P. A. Christensen, T. A. Egerton, J. R. White, *Polym. Degrad. Stab.* **2010**, *95*, 1533.
- [13] T. Konstantinova, A. Bogdanova, S. Stanimirov, H. Konstantinov, *Polym. Degrad. Stab.* **1994**, *43*, 187.
- [14] M. R. Bockstaller, R. A. Mickiewicz, E. L. Thomas, *Adv. Mater.* **2005**, *17*, 1331.
- [15] T. Druffel, N. Mandzy, M. Sunkara, E. Grulke, *Small* **2008**, *4*, 459.
- [16] R. G. DeCorby, N. Ponnampalam, H. T. Nguyen, T. J. Clement, *Adv. Mater.* **2007**, *19*, 193.
- [17] J. R. Castro-Smirnov, M. E. Calvo, H. Míguez, *Adv. Func. Mater.* **2013**, *23*, 2805.
- [18] J. Bailey, J. S. Sharp, *Eur. Phys. J. E* **2010**, *33*, 41.
- [19] J. Bailey, J. S. Sharp, *J. Pol. Sci. B: Pol. Phys.* **2011**, *49*, 732.
- [20] W. Yu, S. Ruan, Y. Long, L. Shen, W. Guo, W. Chen, *Sol. Energy Mater. Sol. Cells* **2014**, *127*, 27.
- [21] W. Yu, L. Shen, P. Shen, Y. Long, H. Sun, W. Chen, S. Ruan, *ACS Appl. Mater. Interfaces* **2014**, *6*, 599.
- [22] P. Zavala-Rivera, K. Channon, V. Nguyen, E. Sivaniah, D. Kabra, R. H. Friend, S. K. Nataraj, S. A. Al-Muhtaseb, A. Hexemer, M. E. Calvo, H. Miguez, *Nat. Mater.* **2012**, *11*, 53.
- [23] M. Lazzari, G. Liu, S. Lecommandoux, *Block Copolymers in Nanoscience*, WILEY-VCH VerlagGmbH&Co., Germany, Weinheim **2006**.
- [24] G. H. Michler, *Electron Microscopy of Polymers*, Springer-Verlag, Berlin, Heidelberg **2008**.
- [25] G. Bernardo, D. Vesely, *Eur. Polymer J.* **2007**, *43*, 4983.
- [26] N. Hidalgo, C. López-López, G. Lozano, M. E. Calvo, H. Míguez, *Langmuir* **2012**, *28*, 13777.
- [27] J. M. Luque-Raigon, J. Halme, H. Miguez, *J. Quant. Spectrosc. Radiat. Trans.* **2014**, *134*, 9.
- [28] E. Nichelatti, *J. Opt. A: Pure Appl. Opt.* **2002**, *4*, 400.
- [29] W. Joo, M. S. Park, J. K. Kim, *Langmuir* **2006**, *22*, 7960.
- [30] R. Núñez-Lozano, B. Pimentel, J. R. Castro-Smirnov, M. E. Calvo, H. Míguez, G. de la Cueva-Mendez, *Adv. Healthc. Mater.* **2015**, DOI: 10.1002/adhm.201500223.
- [31] H. Ikehata, S. Higashi, S. Nakamura, Y. Daigaku, Y. Furusawa, Y. Kamei, M. Watanabe, K. Yamamoto, K. Hieda, N. Munakata, T. Ono, *J. Invest. Dermatol.* **2013**, *133*, 1850.